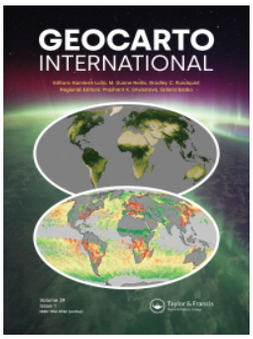

Geocarto International

ISSN: (Print) (Online) Journal homepage: www.tandfonline.com/journals/tgei20

# Sentinel-2 satellite images for monitoring cattle slurry and digestate spreading on emerging wheat crop: a field spectroscopy experiment

Maxence Dodin, Florent Levavasseur, Antoine Savoie, Lucie Martin, Jean Foulon & Emmanuelle Vaudour

**To cite this article:** Maxence Dodin, Florent Levavasseur, Antoine Savoie, Lucie Martin, Jean Foulon & Emmanuelle Vaudour (2023) Sentinel-2 satellite images for monitoring cattle slurry and digestate spreading on emerging wheat crop: a field spectroscopy experiment, Geocarto International, 38:1, 2245371, DOI: 10.1080/10106049.2023.2245371

**To link to this article:** https://doi.org/10.1080/10106049.2023.2245371

GEOCARTO INTERNATIONAL
2023, VOL. 38, NO. 1, 2245371
https://doi.org/10.1080/10106049.2023.2245371

Taylor & Francis
Taylor & Francis Group



# Sentinel-2 satellite images for monitoring cattle slurry and digestate spreading on emerging wheat crop: a field spectroscopy experiment

Maxence Dodin[a], Florent Levavasseur[a], Antoine Savoie[b], Lucie Martin[a], Jean Foulon[b] and Emmanuelle Vaudour[a]

[a]Université Paris-Saclay, INRAE, AgroParisTech, UMR EcoSys, Palaiseau, France; [b]INRAE, UE PAO, Nouzilly, France

**ABSTRACT**

This study is aimed to evaluate the utility of Sentinel-2 imagery for monitoring exogenous organic matter (EOM) applied on winter wheat crop, using two spatial scales: proximal and satellite. From proximal sensing, multi-temporal spectral field measurements were taken on experimental fields consisting of three treatments (cattle slurry, liquid and raw digestates) and a control throughout 46 days. From Sentinel-2 satellites, images were analysed before and after EOM application. For both sensing scales, EOM and vegetation indices were used. On any scale of observation, the digestates spread on emerging wheat were easily detectable in late winter, in contrast to spring spreading events which were hindered by the developed vegetation. The agglomerative hierarchical clustering from the EOM indices divided by EVI achieved to discriminate digestates at early and medium stages of vegetation growth. Our findings did not apply for cattle slurry, presumably because of both lower organic and dry matter contents.

**HIGHLIGHTS**

- Digestates spread on emerging wheat are detectable in late winter.
- Developed vegetation constrains the detection of spring spreading events.
- Spectral measurements did not separate the field with cattle slurry and the control.
- The visible to near infrared bands are the most impacted after digestate spreading.

**ARTICLE HISTORY**
Received 28 March 2023
Accepted 2 August 2023

**KEYWORDS**
Remote sensing; exogenous organic matter; spectral measurement; organic fertilizer; winter wheat

**CONTACT** Maxence Dodin maxence.dodin@inrae.fr

Supplemental data for this article can be accessed online at https://doi.org/10.1080/10106049.2023.2245371.

## 1. Introduction

The application of Exogenous Organic Matter (EOM) in agriculture is a widespread practice which allows the recycling of agricultural, industrial or urban wastes. EOM applications increase soil fertility (Diacono and Montemurro 2010; Chen et al. 2022), but may have negative impacts, such as soil contamination with microplastics (Zhang et al. 2022) or N losses (Maris et al. 2021). Hence the need to monitor this practice, all the more than little is known about the spatial allocation of EOM spreadings.

Anaerobic digestion is a waste transformation process that has been steadily developing since the 2000s (Scarlat et al. 2018). This treatment leads to producing renewable energy (biogas). The residual material is the raw digestate, which can be divided into liquid and solid fractions *via* phase separation. The characteristics of the digestate depend on the process and the feedstock (Guilayn et al. 2019a), which further condition its effects when applied to soil (Möller 2015). Furthermore, various studies have shown the interest of raw or liquid digestates applied either on bare soil before crop sowing or directly on the crop active vegetation to substitute synthetic nitrogen fertilizers (Barłóg et al. 2020; Pastorelli et al. 2021).

Information about the occurrence and frequency of EOM spreadings is required to better understand their impacts at the landscape scale (Tang et al. 2006; Duretz et al. 2011). So far, the procedure of tracking EOM applications consists of surveying farmers but could be supported by remote sensing technology, which is an effective method for monitoring agricultural practices (e.g. Calcagno et al. 2022), water content for precision irrigation (e.g. Romano et al. 2023) or crops (e.g. Bégué et al. 2018; Rivas et al. 2021; Abubakar et al. 2023). However, the spectral behaviour of EOMs is not well-known. A few studies have examined the spectral behaviour of EOMs in lab conditions, either for grape marc compost and liquid cattle manure compost (Ben-Dor 1997), or for hog manure (Malley et al. 2002) or even for cattle and poultry manures in liquid or solid form (Gogé et al. 2021).

Relying on Sentinel-2 satellite time series with weekly revisit and medium spatial resolution (10–20 m), which are likely to target specific dates of amendment spreadings, a few recent studies have addressed the satellite-based monitoring of EOM applications (Dodin et al. 2021; Shea et al. 2022; Pedrayes et al. 2023). Relying on field spectral measurements, Dodin et al. (2021) monitored the spectral behaviour of EOMs spread on bare soil and related it to Sentinel-2 imagery.

Similar organic compounds are observed in both SOC, exogenous organic matters and crop residues (Malley and Martin 2003; Réveillé et al. 2003; Jouraiphy et al. 2005; Lashermes et al. 2009). Furthermore, SOC and EOMs spectra tend to reflect lowly in the visible wavelength (Ben-Dor 2002; Vergnoux et al. 2009; Ogen et al. 2018; Dodin et al. 2021). Dodin et al. (2021) have used such characteristics of EOM to develop spectral indices, named EOMI, for the detection of EOM application. These indices use either red (B4), near-infrared (NIR, B8) or shortwave infrared (SWIR, B11 and B12) spectral bands.

Because EOMs are composed of dead tissues, their spectra are not impacted in a similar manner as active vegetation for which pigmentation strongly absorbs in red and blue regions while highly reflecting in infrared wavelengths (Verhoeven and Loenders 2006). EOMs might be either in solid or in liquid form. In contrast to solid EOM application on bare soils, liquid EOMs applied on crop active vegetation are usually not buried which could ease their detection shortly after spreading. Whatever the form of EOM, be it solid or liquid, the influence that growing crop and/or the drying of liquid EOMs may have on EOM detection has never been studied. Due to crop growth, it requires spectral measurements with weekly revisit time. Our study aims are twofold: (i) spectrally characterize

EOM spreading on emerging vegetation, particularly in liquid form; (ii) assess the capability of Sentinel-2 satellite series for such monitoring. Therefore, this study was led on two scales: firstly, using field spectral measurements to characterize the spectral behaviour of EOM × partially vegetated soils over time and secondly, using Sentinel-2 satellite images to extrapolate field measurements.

## 2. Materials and methods

The global method is described in Figure 1: changes in spectral behaviour of partially vegetated soils fertilized with EOM were studied over time both from Sentinel-2 images and field reflectance measurements over a 46-day period. In order to compare field and image spectra, Sentinel-2 images were chosen as close as possible to the very dates of field measurements.

### 2.1. Study site and farm description

Reflectance measurements were repeatedly carried out within four agricultural fields of the INRAE's experimental unit, located in Nouzilly, France (47°32′27.2″N, 0°47′32.3″E), almost each week from February to April 2022 (Figure A.1). The climate of this region is oceanic with a mean annual temperature of 11.7 °C and a total yearly rainfall of 670 mm. Daily relative air moisture and rainfall during the experiment were collected from a local meteorological station and additional data from Météo France (SAFRAN) (Figure A.1). The experimental unit is a crop-livestock farm with dairy cattle. Since 2014, the farm has been operating an anaerobic digester with a continuous wet mesophilic process which treats 7 500 tons (fresh weight) of wastes per year, composed of cattle slurry (11%), manure (17%), sewage sludge (29%), water runoff (9%), agro-industrial wastes (18%), cereal middlings (8%) and grease (8%). The total retention time is around 100 days in the two digesters (main and post-digester) and at the output, the raw digestate is post-treated with phase separation using a screw press.

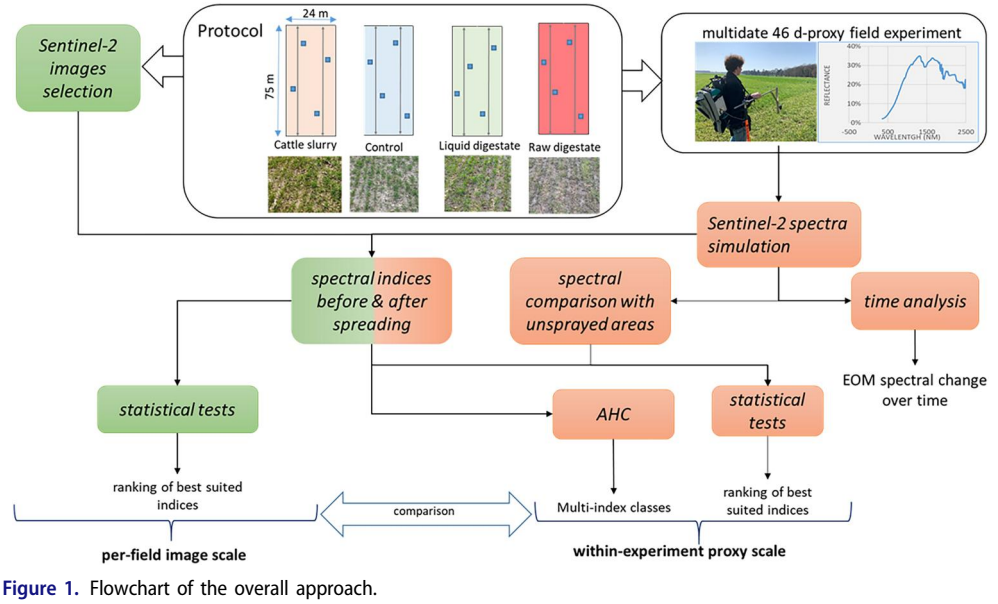


Figure 1. Flowchart of the overall approach.

Our experimentation used an experimental device called 'MétaMetha' (Pasquier et al. 2019; Moinard et al. 2021) started in 2017 and dedicated to the study of digestate spreading in comparison to non-digested manures and mineral fertilization (Figure 2). The crop succession includes rapeseed and cereals and the field is cultivated under conventional management with soil tillage and pesticide use. The field pertains two main soilscape units (Pasquier et al. 2019), composed of a Stagnic Luvisol in the main part and a Haplic Planosol (WRB 2015) in the remaining. The experiment compares five fertilization systems on five plots of 24 × 75 m (one plot per treatment).

The five treatments consisted of the following: fertilization with only mineral N solution (Ctr) in late winter and spring; fertilization with cattle slurry (Slu) in late winter and spring and cattle manure in summer; spreading of raw digestate (Raw_D) in summer, late winter and spring; application of liquid digestate (Liq_D) in late winter and spring and solid digestate in summer, (0 N) without any mineral N fertilization and without any organic amendment. In our study, we focused on the first four treatments (0 N excluded) and on the application of EOM spread in late winter and spring on wheat in 2022 (Figure 3).

The 'MétaMetha' device is relevant for comparing different EOMs for a given soil type- × crop combination. However, the fertilization history of each plot and their layout could bring biases in the reflectance spectra. This is the reason why, in our device, we kept a control area deprived of any spreading for each EOM treatment, which was an area of 12 $m^2$ kept without any EOM left by means of a plastic sheet set prior to the spreading (Figure 3b).

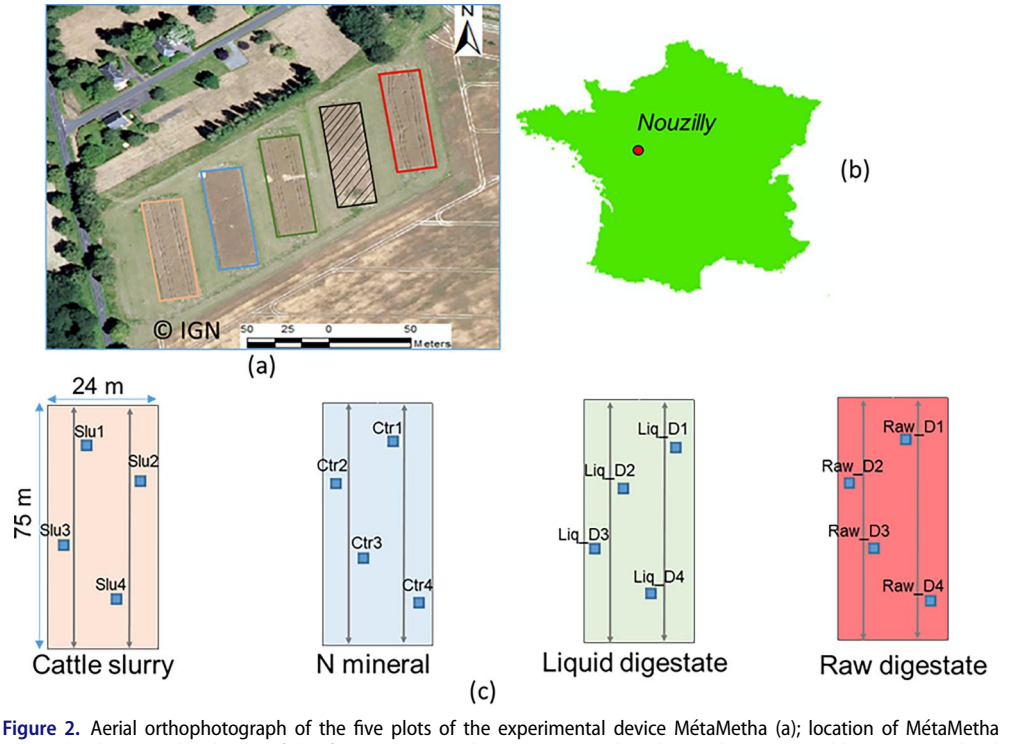


**Figure 2.** Aerial orthophotograph of the five plots of the experimental device MétaMetha (a); location of MétaMetha in mainland France (b); design of the four experimental treatments used in this study (c). Beige, blue, green and red fields represent, respectively, wheat field with application of cattle slurry (Slu), mineral nitrogen (Ctr), liquid digestate (liq_D) and raw digestate (raw_D). Each blue square represents a spectral measurement zone.

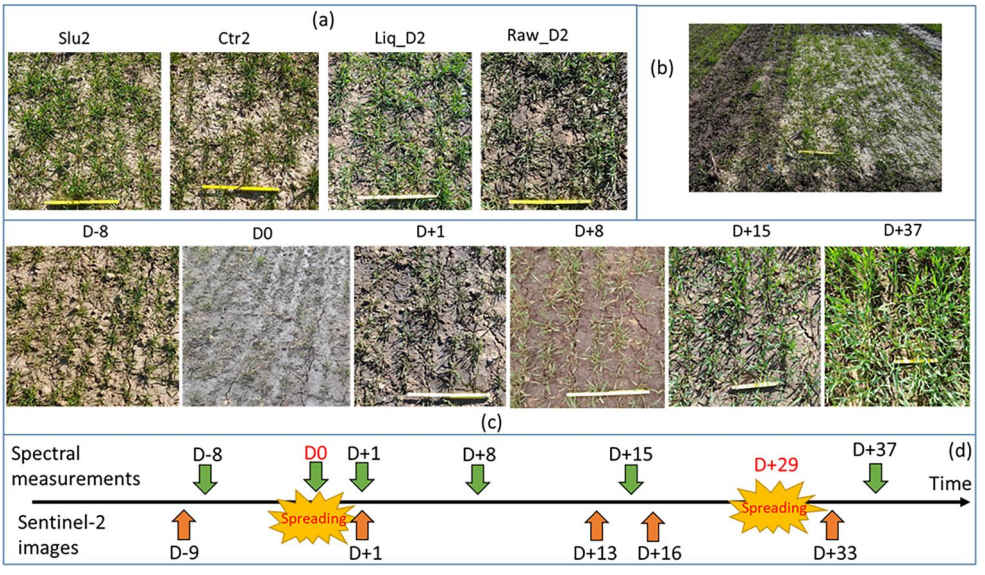


**Figure 3.** Photographs showing the soil surface condition for: (a) cattle slurry (Slu2), control (Ctr2), liquid digestate (liq_D2) and raw digestate (raw_D2) on March 9th 2022 ($D+1$);(b) the area without digestate into raw digestate field; (c) and their evolution during the experimentation for the raw digestate 1 area (raw_D1), from left to right 8 days before EOM application, the day of application, one day, eight days, 15 days and 37 days after spreading. Then, (d) chronology of spectral measurements carried out and Sentinel-2 images used.

**Table 1.** Main characteristics of the spread EOMs. RM and DM mean raw matter and dry matter, respectively.

| EOM (Standards) | Spread quantity (t/ha) | DM (% RM) (NF EN 12880) | Organic matter (g OM $kg^{-1}$ RM) (NF EN 13039) | Total N (g N $kg^{-1}$ RM) (NF EN 13654-2) | $N\text{-}NH_4$ (g N $kg^{-1}$ RM) (NF X 31-130) | Organic C/N ratio |
|---|---|---|---|---|---|---|
| Cattle slurry 8th March 2022 | 26.75 | 1.23 | 9.74 | 1.17 | 0.26 | 9 |
| Liquid digestate 8th March 2022 | 26.51 | 6.41 | 44.29 | 1.95 | 1.22 | 4.9 |
| Raw digestate 8th March 2022 | 31.63 | 8.77 | 64.46 | 1.82 | 1.0 | 7.3 |
| Cattle slurry 6th April 2022 | 43.25 | 3.78 | 31.22 | 1.22 | 0.47 | 9.1 |
| Liquid digestate 6th April 2022 | 37.57 | 6.9 | 49.40 | 3.14 | 1.15 | 7.2 |
| Raw digestate 6th April 2022 | 24.86 | 9.22 | 69.61 | 1.89 | 1.62 | 9.2 |

The standards for the methods used are indicated in brackets.

The EOMs were sampled for analysis in a lab, at the time of application (Table 1). All EOMs used for this experimentation originated from the experimental farm of Nouzilly and were applied using a trailing hose. The synthetic fertilizer was a solution with 30% N (15% urea, 7.5% ammonium and 7.5% nitrate). The global compositions of raw and liquid digestates were quite similar compared to the cattle slurry spread in late winter, which was diluted. However, due to the process of phase separation (screw press system), the raw digestate had a higher content of dry matter than liquid digestate. Referring to the ammonium form of mineral nitrogen fraction of EOMs spread per hectare, the digestate inputs were fairly similar whereas cattle slurry was lower, in part due to an ammonia content lower than expected for the first spreading. Such difference is even more marked for the organic matter content of the cattle slurry compared to digestates during the first application. The N rate was determined in function of winter wheat yield objectives, soil mineral nitrogen (SMN) available in late winter, and crop N uptake in late winter. The EOM rate was then determined depending on the N rate and the available N content of

EOM. Following usual fertilization practices for wheat, EOM rate was split into two separate applications in late winter then early spring. The very dates of application were adjusted according to weather conditions. The first EOM spreading occurred on 8th March 2022, designated as day 0 (D0) of the study, while the second spreading was on 6th April 2022, referred as day 29 ($D+29$) of the experiment.

### 2.2. Field reflectance measurement

Repeated spectral measurements of EOM applications were conducted on emerging winter wheat crop within the 'MétaMetha' device, at six dates: 28th February (D-8), 8th, 9th, 16th, 23rd March (D0, $D+1$, $D+8$, $D+15$) and 14th April ($D+37$) 2022 (Figure 3d). For each field, four 2 m × 2 m square areas were evenly defined within each treatment in order to account for its spatial heterogeneity. For each treatment with EOM application, an area was kept left of any EOM using black plastic tarp to protect the soil during the EOM spreading, in order to compare the difference in spectral reflectance between spread and non-spread crop, over the curse of the experiment (Figure 3b). Such 'non-spray areas' are not specified on Figure 2c because their GPS points were not recorded. However, they were located towards the centre of the fields to avoid any border effect. The reflectance of these non- spray areas was measured one day after spreading for raw digestate and both 15 and 37 days ($D+15$, $D+37$) after the first EOM spreading for all EOM treatments (Figure 3d).

Spectral measurements were performed with FieldSpec®3 (Analytical Spectral Devices Inc., Boulder, CO, USA) portable spectroradiometer with the following characteristics: a 350–2500 nm spectral range; a spectral resolution of 3 nm in the 350–1000 nm region (sampling interval 1.4 nm) and 10 nm in the 1000–2500 nm region (sampling interval 2 nm); a 25° field of view; each reflectance measurement at a 0.8 m-height integrating a spot size of about 0.1 $m^2$ at nadir. In order to minimize variations in illumination conditions and shadow effects related to vegetation, the measurements were taken under conditions of few cumulus clouds between ± 2h around solar noon (solar noon times were 13:07 and 13:39 at the start and the end of the experimentation respectively, in local French time). However, the spectral measurements eight days after EOM application were taken under homogenous cloud conditions. Each field measurement was repeated by moving the spectroradiometer inside each 2 m × 2 m square area. The values used at each spectral measurement area were the average of 60–70 spectra calibrated against a 30 cm × 30 cm Spectralon® reflectance panel.

### 2.3. Satellite image reflectance spectra

The Sentinel-2 satellites acquire images from a Multispectral Instrument (MSI) sensor in the visible to shortwave infrared spectral ranges. Five Sentinel-2 images acquired during field measurement campaign were downloaded from the Théia French land data center (THEIA-LAND, 2022), which provides ten spectral bands with 10 m (B2, B3, B4 and B8) or 20 m (B5, B6, B7, B8A, B11 and B12) spatial resolution. The experimental fields were observed from two relative orbits (number 51 and 94) of Sentinel-2, providing more frequent images. These images were already ortho-rectified and atmospherically corrected with the MACCS-ATCOR Joint Algorithm (MAJA) processor (Baetens et al. 2019). A mask of cloud and their shadows ('*masque géophysique*', MG2 mask), also provided by Théia, was used. All spectral bands with 20 m spatial resolution were resampled to 10 m. Thus, between 16 and 19 pixels were extracted for each treatment. The closest acquisition

**Table 2.** Characteristics of the Sentinel-2 satellite acquisitions.

| Acquisition date | Day of experimentation | Satellite | Relative orbit number | Cloud cover (%) | Rainfall day of acquisition (mm) | Cumulative rainfall 3 days before acquisition (mm) | Cumulative rainfall 7 days before acquisition (mm) |
|---|---|---|---|---|---|---|---|
| 27th February 2022 | D-9 | S2B | 94 | 0 | 0 | 1.8 | 4 |
| 9th March 2022 | $D+1$ | S2B | 94 | 36 | 0 | 0 | 0.4 |
| 21st March 2022 | $D+13$ | S2A | 51 | 57 | 0.4 | 1 | 3.6 |
| 24th March 2022 | $D+16$ | S2A | 94 | 0 | 0 | 0.4 | 1 |
| 10th April 2022 | $D+33$ | S2A | 51 | 45 | 0 | 22.2 | 22.2 |

dates were comprised between 1 and 4 days before and after field measurement (Table 2). No rainfall occurred at images acquisition dates and within the period of field campaign.

### 2.4. Spectral indices for EOM detection

In total seven spectral indices were computed. EOMI1, EOMI2, EOMI3, EOMI4 and NBR2 (Equations 1–5) were previously proposed to monitor EOM amendment by Dodin et al. (2021). EOMI3 (Equation 3) combines EOMI1 and EOMI2 and use the red, NIR and SWIR bands of Sentinel-2 most impacted by solid EOM (Dodin et al. 2021). In order to consider winter wheat vegetation, EVI and NDVI have also been used. Finally, ratios between EOM indices and vegetation indices were elaborated to account for the growing vegetation and the spreading of EOM together.

$$\mathrm{EOMI1} = (\mathrm{B11}-\mathrm{B8A})/(\mathrm{B11}+\mathrm{B8A}) \quad (1)$$

$$\mathrm{EOMI2} = (\mathrm{B12}-\mathrm{B4})/(\mathrm{B12}+\mathrm{B4}) \quad (2)$$

$$\mathrm{EOMI3} = ((\mathrm{B11}-\mathrm{B8A})+(\mathrm{B12}-\mathrm{B4}))/(\mathrm{B11}+\mathrm{B8A}+\mathrm{B12}+\mathrm{B4}) \quad (3)$$

$$\mathrm{EOMI4} = (\mathrm{B11}-\mathrm{B4})/(\mathrm{B11}+\mathrm{B4}) \quad (4)$$

$$\mathrm{NBR2} = (\mathrm{B11}-\mathrm{B12})/(\mathrm{B11}+\mathrm{B12}) \quad (5)$$

$$\mathrm{NDVI} = (\mathrm{B8}-\mathrm{B4})/(\mathrm{B8}+\mathrm{B4}) \quad (6)$$

$$\mathrm{EVI} = 2.5*(\mathrm{B8}-\mathrm{B4})/(\mathrm{B8}+\mathrm{B4}*6-\mathrm{B2}*7.5+1) \quad (7)$$

where B2 (458–523 nm), B4 (650–680 nm), B8 (785–899 nm), B8A (855–875 nm), B11 (1565–1655 nm) and B12 (2100–2280 nm) refer to the Sentinel-2 spectral bands.

### 2.5. Analysis of field reflectance spectra and temporal indices profiles

Field spectral measurements of each area were acquired before and after EOM applications, and compared, in order to understand the spectral response according to EOMs and over time. Moreover, for some dates, we compared within-fields 'non-spray areas' and 'spray areas' for cattle slurry and digestates with control field. Regardless of EOM or wheat vegetation, this ensured that differences in spectral reflectance between treatments were not due to differences in soil reflectance.

Then, EOM and vegetation indices were calculated from the simulated Sentinel-2 spectra. Both ANOVA and Tukey tests, with a 99% confidence interval, were applied on spectra and indices (Table 3). In case ANOVA's conditions were not satisfied, both Kruskal-Wallis and Conovor-Iman test, with a 95% confidence interval, were applied.

Moreover, an Ascending Hierarchical Clustering (AHC) with the Ward method (Ward 1963) was calculated, on either the simulated Sentinel-2 spectra, or the spectral indices.

Table 3. Variables used in statistical tests for each type of studied data.

| Data studied | Days | Repetitions | Variables |
|---|---|---|---|
| Field spectral measurements before EOM spreading | D-8 | 6 spectra for each spectral area | Reflectance (10 bands)<br>NDVI or EVI |
| Field spectral measurements before and after spreading | D-8 and $D+1$ | 4 areas per treatment (spectral measurement areas) | Reflectance (10 bands) |
| Field spectral measurements | All | 4 areas per treatment (spectral measurement areas) | All indices<br>EOM indices divided by EVI or NDVI |
| Field spectral measurements of areas without EOM | All | 6 spectra for each spectral area | Reflectance (10 bands) |
| Sentinel-2 images | All | Between 17 and 19 pixels per treatment | Reflectance (10 bands)<br>All indices |

The clustering was realized from the several following datasets: (i) the 32 simulated Sentinel-2 spectra of the 4 treatments × 4 field spectral measurement areas before and after each spreading date; (ii) the 24 simulated Sentinel-2 spectra for the same treatment over time (4 spectral measurement areas of either the control or the EOM treatment × 6 days); (iii) all indices of 96 observations (4 spectral measurement areas × 4 treatments × 6 days), for the purpose of observing their evolution over time; (iv) five selected EOM indices divided by either EVI or NDVI for 96 observations (4 spectral measurement areas × 4 treatments × 6 days).

## 3. Results

### 3.1. Analysis of field spectra before and just after EOM spreading

Eight days before EOM application, soil reflectance measurements acquired on winter wheat vegetation exhibited a slight heterogeneity of green vegetation amongst measurements areas (Figure A.2). Such difference in NDVI values was confirmed by ANOVA tests, applied to the simulated Sentinel-2 spectral bands, which indicate differences between treatments for the B2 to B5 and B11 bands, 8 days before EOM spreading (Table A.1). Tukey tests showed a significant difference in reflectance, before EOM spreading, between control and raw digestate treatment, at $\alpha = 0.01$, for the B3, B5 and B11 bands and between raw digestate field and liquid digestate field for the B4 band (Table A.1).

Differences between spectra are illustrated before and just one day after EOM spreading, so as to limit the possible impact of moisture change due to either evaporation of the liquid EOMs, or rainfall event, that were likely to occur more than one day after EOM spreading (Figure 4). For both raw and liquid digestate treatment after EOM spreading, the simulated Sentinel-2 spectra showed a significant decrease ($\alpha = 0.01$) in reflectance for all the spectral bands, except for the B11 and B12 bands, compared to the values before spreading (Table A.2). The decrease in reflectance was higher for raw digestate, compared to liquid digestate. Compared to its reflectance before spreading, the slurry treatment only exhibited significant decrease (at $\alpha = 0.01$) for the B8 and B8A bands. Whatever the spectral band, the control treatment showed no significant difference compared to its reflectance eight days earlier. Moreover, one day after application, the three EOM treatments showed a significant decrease of reflectance for all bands, compared to the control treatment, except for the B6, B7, B8 and B8A bands for the slurry treatment. Whereas raw digestate showed no significant difference with liquid digestate for the visible (B2 to B4) and SWIR (B11 and B12) bands after spreading, the slurry treatment had reflectance spectra closer to before-spreading.

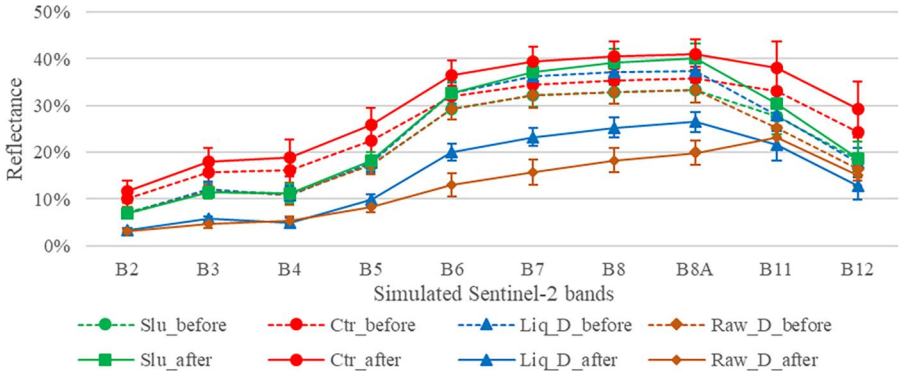


**Figure 4.** Simulated Sentinel-2 reflectance spectra eight days before EOM application (dotted line) and one day after EOM spreading (full line) according to treatment.

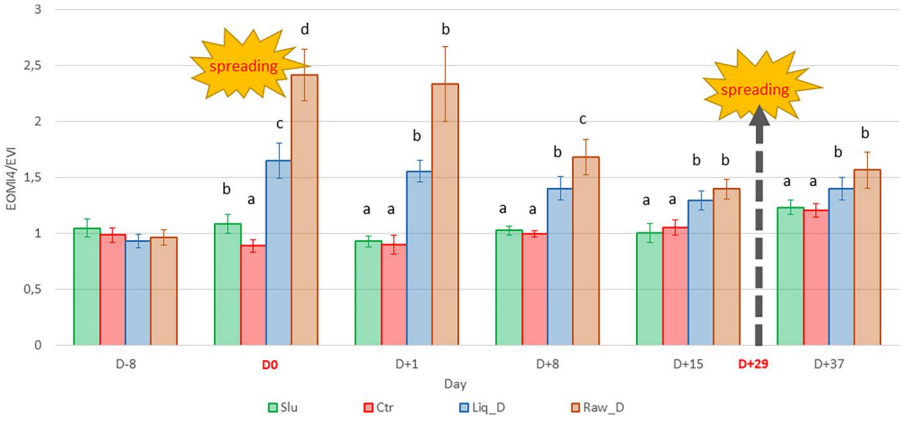


**Figure 5.** Temporal changes of the ratio EOMI4:EVI, calculated from field spectral measurements, for all treatments. Error bars represent the standard deviation of the spectra measured for each treatment. Slu, Ctr, liq_D and raw_D refer to cattle slurry, mineral nitrogen, liquid digestate and raw digestate respectively. For each day, different letters indicate that the treatments showed significant differences ($p < 0.05$) using Conover-Iman test. No letter indicates that there was no significant difference between the treatments ($p > 0.05$).

### 3.2. Analysis of spectral changes in the field experiment over the 46 days period

To account for both growing vegetation and EOM spreading, all indices were expressed in function of either EVI or NDVI. As the ratio EOMI4:EVI appeared to be relevant, Kruskal-Wallis test was applied to analyze its temporal changes according to each treatment (Figure 5 and Table A.3). The treatments did not spectrally differ before spreading: no significant differences between control and the EOM treatments were observed at D-8. All EOMs could be significantly discriminated at $\alpha = 0.05$ between not only the control but also between each other on the very day of their spreading D0. For the measurements performed up to 37 days after the first spreading ($D + 37$), only raw and liquid digestates showed a lingering significant difference compared to control.

### 3.3. Spectral impact of EOMs for each treatment: comparison with unsprayed areas

A significant difference in reflectance between raw digestate and the non-spray spectral areas was found one day ($D + 1$) and 15 days ($D + 15$) after spreading, through a

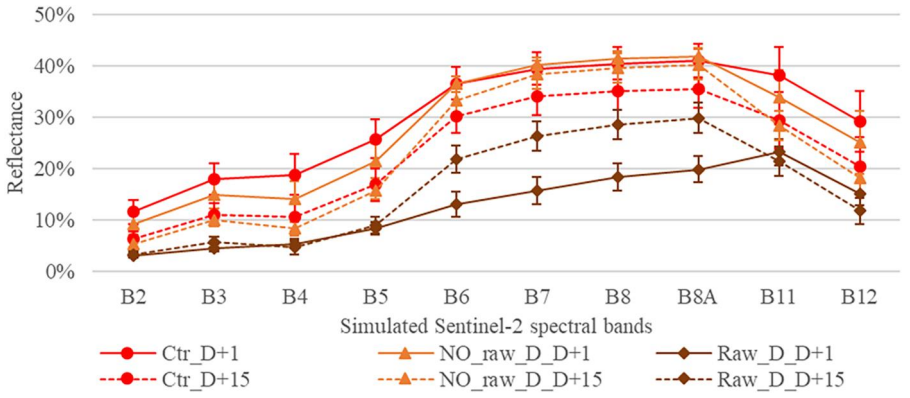


**Figure 6.** Simulated Sentinel-2 reflectance spectra for one day after (full line) and 15 days after (dotted line) raw digestate spreading. Control (Ctr), raw digestate treatment (raw_D) and the area without digestate within the raw digestate field (NO_raw_D) are respectively in red, brown and orange.

Kruskal-Wallis test with 95% confidence level. For all simulated spectral bands (Figure 6, Tables A.4 and A.5). As expectable, there was no difference between the non-spray area within raw digestate treatment and the control areas for B6, B11 and B12 bands. However, slight significant differences appeared one day after the first application for the B2 to B5 bands and B7 to B8A bands between the non-spray area and respectively the Ctr3 and the Ctr1 areas (Table A.4), which may be due to soil variability. These results were nearly the same fifteen days after the first application (Table A.5).

Fifteen days after the first EOM spreading ($D+15$), a significant difference was persisting between liquid digestate spectral areas and the non-spray area for almost all bands, except for B8A and B8 (Table A.6). Significant differences between control and raw and liquid digestate were also visible but quite variable for B7 to B12 and B6 to B11, depending on the spectral measurement areas.

### 3.4. Multi-indices grouping of the EOMs according to type

The AHC results obtained from the five spectral indices focused on organic matter (EOMI1, 2, 3, 4 and NBR2) divided by EVI and computed for all field spectra are displayed on Figure 7. Four classes were obtained, that successfully discern between levels of EOM application. Class 1 groups all treatments before spreading (D-8) and both control and cattle slurry treatments until 15 days after spreading. Class 2 gathers both liquid and raw digestate treatments between eight and 15 days after spreading, in addition to the early days of spreading (D0, $D+1$) for liquid digestate specifically. Class 3 includes the raw digestate treatment for the day of spreading, one day after application and the area n°1 for the measurements eight days after spreading. Finally, class 4 embraces all treatments 37 days after the first EOM application.

### 3.5. Sentinel-2 image spectra and images indices over the field experiment

Even though the experimental fields were small, they included between 16 and 19 pixels of 10 m spatial resolution per treatment: we managed to monitor them from Sentinel-2 images (Figure 8). The image reflectance spectra exhibited an important decrease between the control and the raw digestate treatments for B2 to B6 bands and for the B8 band until sixteen days after the first EOM spreading (Figure 9). Such decrease one day after the first

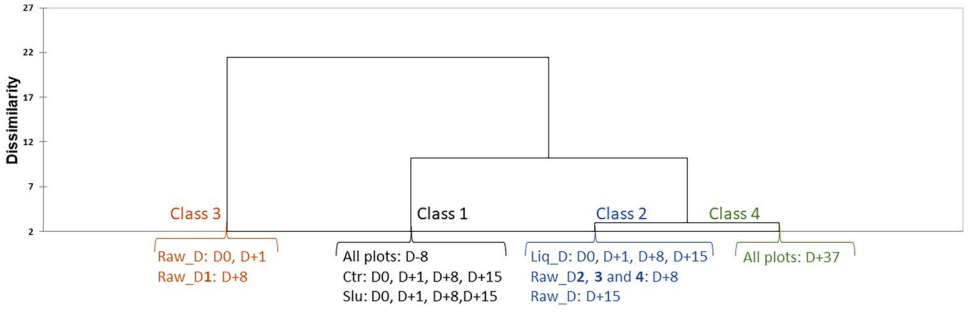


**Figure 7.** AHC Dendrogram from the five EOM indices (EOMI1 to 4 and NBR2) divided by EVI for all treatments, over time. Number of the spectral measurement areas are indicated in bold when all areas of the same treatment and at the same date are not in the same class. Classes 1, 2, 3 and 4 in black, blue, brown and green colors, respectively.

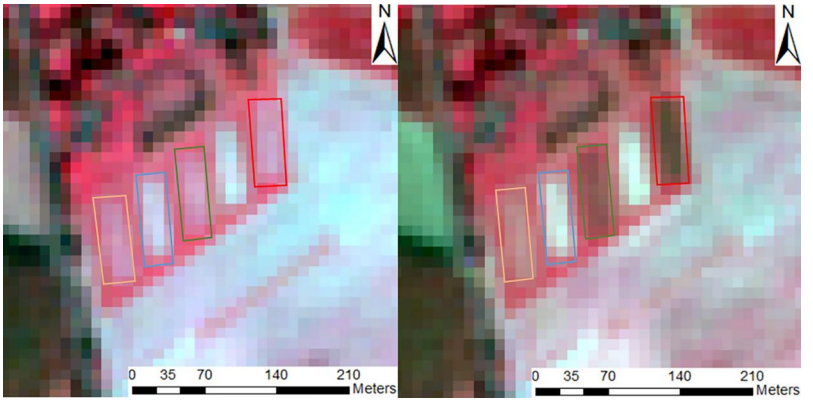


**Figure 8.** Infrared colored composite images (R:B8, G:B4, B: B3) nine days before spreading (left) and one day after EOM application. Beige, blue, green and red fields represent, respectively, wheat field with application of cattle slurry (Slu), mineral nitrogen (Ctr), liquid digestate (liq_D) and raw digestate (raw_D).

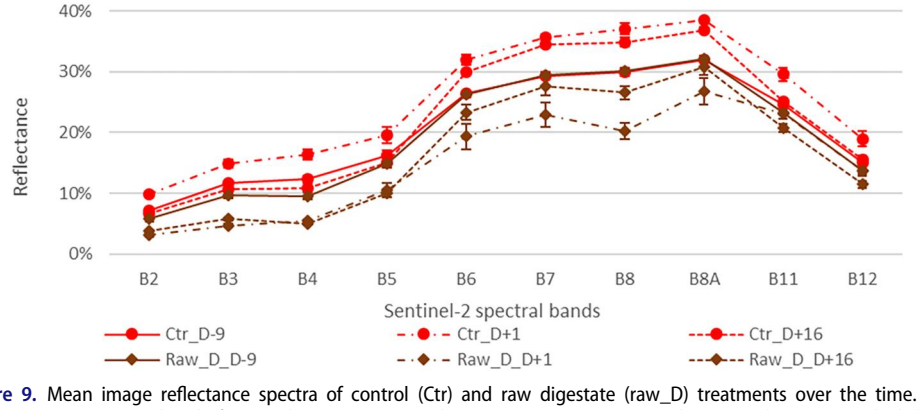


**Figure 9.** Mean image reflectance spectra of control (Ctr) and raw digestate (raw_D) treatments over the time. The date 27/02 (D-9) was taken before application. 09/03 and 24/03 represent, respectively, Sentinel-2 images which have been taken one day ($D+1$) and 16 days ($D+16$) after spreading.

application was less marked for liquid than for raw digestate (Table A.7). At $D+16$, the post-spreading decrease in reflectance can only be observed for the B2 to B5 bands for liquid digestate. Slurry treatment showed only an increase of reflectance for the B6 to B8A bands after application compared to its spectra before application (Table A.7).

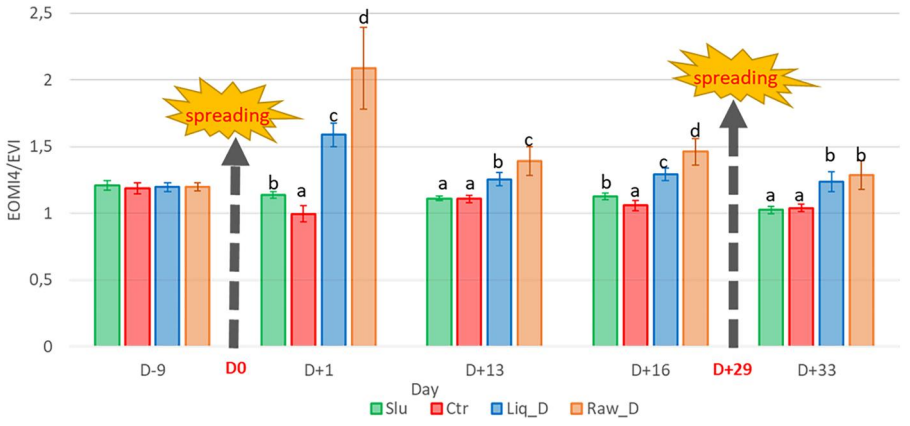


**Figure 10.** Temporal changes of the ratio EOMI4:EVI, calculated from Sentinel-2 spectral bands, for all treatments. Error bars represent the standard deviation of the pixels on each treatment. Slu, Ctr, liq_D and raw_D respectively refer to cattle slurry, mineral nitrogen, liquid digestate and raw digestate plot. For each day, different letters indicate that the treatments showed significant differences ($p < 0.05$) using Conover-Iman test. The absence of letters indicates that there was no significant difference between the treatments ($p > 0.05$).

Field spectral measurements showed that EOM indices divided by EVI might be relevant to monitor EOM spreading on vegetation from Sentinel-2 images. Indeed, the EOMI4:EVI ratio records temporal changes marked by an increase after EOM spreading for digestate treatments compared to both before spreading treatments and control (Figure 10). Moreover, temporal changes of this ratio for the cattle slurry treatment after spreading confirm difficulties to differentiate between it and both control and fields before spreading.

## 4. Discussion

### *4.1. Feasibility of liquid EOM application detection with simulated Sentinel-2 spectra*

Little is known about the spectral behaviour of several EOMs, especially liquid manure and digestates, be it spread on bare soil or on vegetated soil. This research pioneers the mapping of liquid EOM practices spread on winter wheat crop from optical satellite images. Spectral measurements in the field contribute to better understand spectral trends of liquid EOMs spread on vegetation and offer a basis for developing appropriate spectral indices. Our study demonstrates that: (i) digestates spread on emerging wheat are easily detectable in late winter, and this as long as 15 days after spreading; (ii) the visible to near infrared simulated spectral bands (B2 to B8A) are the most influential during the first days after spreading, the B2 to B4 and B5 having persisting impact 15 days after; (iii) winter wheat above 23 cm limits the detection of spring applications.

This study confirms previous study focused either on a bare cropland field (NDVI $<$ 0.35) (Dodin et al. 2021) or pasture (Pedrayes et al. 2023), tracking modifications of the field reflectance due to the spreading of solid EOM amendment. Currently, access to precise dates of liquid EOM spreading on crop relies upon fastidious surveys of farmers. It is worth mentioning that the knowledge provided in this study brings complementary information that could serve satellite-based approaches of topsoil SOC prediction (Vaudour et al. 2022, Žížala et al. 2022), tillage practices (e.g. Vaudour et al. 2015), crop monitoring (e.g. Rivas et al. 2021), or irrigation (e.g. Elwan et al. 2022).

Nevertheless, it's worth mentioning that some field spectral measurements, which could not be done immediately after spring spreading, were carried out as late as 8 days after spring application due to unfavourable weather. There might be a mismatch between optimal conditions for spectral measurements requiring a cloudless weather while a mild cloudy weather without wind is optimum for EOM application needs (Hafner et al. 2018): this could be a hindrance for identifying EOMs spreading from optical satellite series under extended cloudy weather.

### 4.2. A promising tool to monitor digestate spreading on emerging crop

The differences in vegetation height which were prevailing between EOM and control treatments eight days before EOM spreading may have contributed to the observed differences in measured reflectance. Indeed, such differences may be due to the amendment protocol which has been applied since 2017 for this experiment. According to Odlare et al. (2014) and Zicker et al. (2020), the practice of EOM spreading over a period as short as 8 or 9 years can cause an increase in soil organic matter content, hence an enhanced crop development. Still, between plots fertilized with either liquid manure or digestate during 20 years, Wentzel et al. (2015) showed on average no difference in SOM content. Whatever the variations in vegetation growth due to specific fertility conditions in each field, the 'non-spray' areas within EOM treatments confirmed the decrease in reflectance due to digestate application. Subsequently, the vegetation disparity was also mitigated by the use of spectral indices.

Regardless of the slight disparities in vegetation growth at early and medium stages, the AHC clustering from the EOM indices divided by EVI demonstrated their potential for detecting both liquid and raw digestates, but this did no longer hold true for higher levels of active vegetation. Indeed, both spectral measurements carried out at $D+8$ and $D+37$ were done 8 days after EOM application (respectively at D0 and $D+29$), yet the first spreading ($D+8$) only can be distinguished from the control treatment through the AHC results. Between these two dates, the growth of winter wheat was the main difference that could disrupt the monitoring of EOMs.

The differences sensed from the field-based indices subsisted from the Sentinel-2 images acquired throughout the trial period, even though each treatment field was of limited size, comprising less than 20 pixels with 10 meters resolution, some of which were mixels of field bordering vegetation. Given its limited spatial extent, this Sentinel-2-based approach can be seen as a primer for further implementation over larger fields. It's worth noting that in the context of our experiment, most Sentinel-2 bands showing a significant difference between control and raw digestate treatment were those having a spatial resolution of 10 meters. We therefore may expect that Sentinel-2 bands with 20 m spatial resolution, showing here no significant differences after EOM application because the fields were too small, would get better results with larger fields. A further implementation with the BIODIVERSITY sensor with similar revisit frequency and higher spectral and spatial resolutions would be even more recommended (Briottet et al. 2022).

### 4.3. Influence of liquid EOM type and composition

The spectral differences observed on the very day of application (D0) and the next day ($D+1$) may be influenced by EOM moisture. An increase in soil moisture mainly causes a decrease of reflectance around 1400 and 1900 nm (Yu et al. 2022) but also impacts the whole spectrum by a decrease in reflectance (Rienzi et al. 2014). Of course, the spectral variations that were observed through this study cannot be explained by moisture only,

**Table 4.** Dry matter (DM), organic matter (OM) and total nitrogen (N) of the EOMs spread in late winter, expressed per hectare.

| EOM | DM (kg DM $ha^{-1}$) | Organic matter (kg OM $ha^{-1}$) | Total N (kg N $ha^{-1}$) |
|---|---|---|---|
| Cattle slurry 8th March 2022 | 32.9 | 260.6 | 31.2 |
| Liquid digestate 8th March 2022 | 169.9 | 1174.2 | 51.7 |
| Raw digestate 8th March 2022 | 277.4 | 2038.9 | 57.7 |

particularly those referring to digestates, for which the addition of organic matter was obviously influent and visually noticeable in the field (Figure 3) as well as in the Sentinel-2 images (Figure 8). This did not apply for cattle slurry, which was hardly visible even in the field, and even less in the Sentinel-2 images.

Indeed, the ratio EOMI4:EVI did not provide any better result for slurry, and this even one day after the first application, for which the only few significant differences were found for the infrared bands of simulated Sentinel-2 spectra. Whatever the measurement day, the cattle slurry treatment was confused with control through the AHC. A further use of both Sentinel-1 and Sentinel-2 may facilitate the detection of such liquid manure (Shea et al. 2022). However, the failure in detecting slurry spreading from Sentinel-2 data might stem from the fact that it was diluted. It shall be specified that neither composition nor applied quantity were detailed in the study of Shea et al. (2022) for liquid manure. Thus, further studies are needed on a field or landscape scale to compare different compositions and rates of cattle slurry.

By contrast, our study clearly indicates the possibility of monitoring digestate applications, presumably because of their higher content in organic matter and their higher dry matter compared to the diluted slurry which was spread through this experiment (Table 4). Indeed, compared to raw digestate at the first EOM application, the quantity of both dry matter and organic matter spread per hectare for the cattle slurry was 8.4 (277.4 vs 32.9 kg/ha) and 7.8 (2038.9 vs 260.6 kg/ha) times lower, respectively. Thus, based on the composition of cattle slurry spread in the first spreading event, an additional 23 tons per hectare would have been required to obtain the same amount of total nitrogen as the raw digestate, which cannot be reached though the doses used in this territory.

The waste introduced in the anaerobic digester and the digestion process modify organic matter composition, hence the differences in reflectance between slurry and digestate in diverse parts of the spectrum (Ben-Dor 1997). Our study show that raw digestate causes higher reflectance decrease than liquid digestate. This was foreseeable because of the higher organic matter content of raw digestate at the first EOM application: 2038.9 versus 1174.2 kg/ha, respectively, for raw and liquid digestate (Table 4). Another phase separation could also show higher differences between raw and liquid digestates. Furthermore, screw press system, used in this study, exports around 30% of the dry matter to the solid phase, whereas centrifugation system exports around 80% (Guilayn et al. 2019b) and produces a more diluted digestate, which could be more difficult to detect.

## 5. Conclusion

This research pioneers the mapping of liquid EOM practices spread on winter wheat crop from optical remote sensing and especially from satellite images. It demonstrates that digestates spread on emerging wheat are easily detectable in late winter, while developed vegetation limit the detection of spring applications. This detection of spread digestates was favoured by the visible to near infrared bands which are the most impacted during the first days after spreading. The visible to red-edge bands are those persistently

impacted until 15 days after EOM application. This did not apply for cattle slurry, which was hardly visible in the field, presumably because of both lower organic and dry matter contents and was hence even less observable from the Sentinel-2 images. Regardless of the slight disparities in winter wheat growth at early and medium stages, the AHC clustering from the EOM indices divided by EVI demonstrated their separative potential for detecting both liquid and raw digestates, yet this no longer held true for higher levels of active vegetation. Given its limited spatial extent, this Sentinel-2-based approach can be seen as a primer for further implementation over larger fields that would test the feasibility of spatial monitoring at farm level or even across small regions.

## Acknowledgments

We wish to thank Jean-Marc Gilliot for making his recent update of the read.asd tool available, thus enabling us to simulate the MSI spectral bands. Special thanks to the PAO experimental unit team who participated in this experimentation.

## Authors' contributions

Conceptualization, M.D., F.L., A.S., E.V.; data curation, M.D., E.V.; methodology, M.D., F.L., A.S., E.V.; validation, M.D., F.L., E.V.; resources, L.M., J.F.; writing original draft, M.D.; writing-review & editing, M.D., F.L., A.S., L.M., J.F., E.V.; supervision, F.L., E.V.; project administration, E.V.; funding acquisition, E.V.

## Disclosure statement

The authors declare that they have no known competing financial interests or personal relationships that could have appeared to influence the work reported in this article.

## Funding

This work was supported by the European Union's Horizon H2020 research and innovation European Joint Programme Cofund on Agricultural Soil Management (EJP-SOIL Grant Number 862695) and was carried out in the framework of the STEROPES of EJP-SOIL. This work was also supported by CNES, France, in the framework of the POLYPHEME project through the TOSCA program of the CNES (Grant Number 200769/id5126) and the MELICERTES project (ANR-22-PEAE-0010) of the French National Research Agency (France2030 and national PEPR 'agroécologie et numérique' programmes). Maxence Dodin has received the support of a PhD scholarship from the French Ministry of Agriculture.

## ORCID

Florent Levavasseur http://orcid.org/0000-0002-2164-3334
Emmanuelle Vaudour http://orcid.org/0000-0002-4703-3702

## Data availability statement

The data that support the findings of this study are available from the corresponding author, M.D., upon reasonable request.

## References

Abubakar MA, Chanzy A, Flamain F, Pouget G, Courault D. 2023. Delineation of orchard, vineyard, and olive trees based on phenology metrics derived from time series of Sentinel-2. Remote Sens. 15(9): 2420. doi: 10.3390/rs15092420.

Baetens L, Desjardins C, Hagolle O. 2019. Validation of Copernicus Sentinel-2 cloud masks obtained from MAJA, Sen2Cor, and FMask processors using reference cloud masks generated with a supervised active learning procedure. Remote Sens. 11(4):433. doi: 10.3390/rs11040433.

Barłóg P, Hlisnikovský L, Kunzová E. 2020. Yield, content and nutrient uptake by winter wheat and spring barley in response to applications of digestate, cattle slurry and NPK mineral fertilizers. Arch Agron Soil Sci. 66(11):1481–1496. doi: 10.1080/03650340.2019.1676890.

Bégué A, Arvor D, Bellon B, Betbeder J, de Abelleyra D, P. D. Ferraz R, Lebourgeois V, Lelong C, Simões M, R. Verón S. 2018. Remote sensing and cropping practices: a review. Remote Sens. 10(2):99. doi: 10.3390/rs10010099.

Ben-Dor E. 1997. The reflectance spectra of organic matter in the visible near-infrared and short wave infrared region (400–2500 nm) during a controlled decomposition process. Remote Sens Environ. 61(1):1–15. doi: 10.1016/S0034-4257(96)00120-4.

Ben-Dor E. 2002. Quantitative remote sensing of soil properties. In Advances in agronomy, vol. 75; Academic Press: Cambridge, MA, USA; p. 173–243.

Briottet X, Bajjouk T, Chami M, Delacourt C, Féret JB, Jacquemoud S, Minghelli A, Sheeren D, Weber C, Fabre S, et al. 2022. BIODIVERSITY – A new space mission to monitor Earth ecosystems at fine scale. RFPT. 224(1):33–58. doi: 10.52638/rfpt.2022.568.

Calcagno F, Romano E, Furnitto N, Jamali A, Failla S. 2022. Remote sensing monitoring of durum wheat under no tillage practices by means of spectral indices interpretation: a preliminary study. Sustainability. 14(22):15012. doi: 10.3390/su142215012.

Chen H, Levavasseur F, Montenach D, Lollier M, Morel C, Houot S. 2022. An 18-year field experiment to assess how various types of organic waste used at European regulatory rates sustain crop yields and C, N, P, and K dynamics in a French calcareous soil. Soil Tillage Res. 221:105415. doi: 10.1016/j.still.2022.105415.

Diacono M, Montemurro F. 2010. Long-term effects of organic amendments on soil fertility. A review. Agron Sustain Dev. 30(2):401–422. doi: 10.1051/agro/2009040.

Dodin M, Smith HD, Levavasseur F, Hadjar D, Houot S, Vaudour E. 2021. Potential of Sentinel-2 satellite images for monitoring green waste compost and manure amendments in temperate cropland. Remote Sens. 13(9):1616. doi: 10.3390/rs13091616.

Duretz S, Drouet JL, Durand P, Hutchings NJ, Theobald MR, Salmon-Monviola J, Dragosits U, Maury O, Sutton MA, Cellier P. 2011. NitroScape: a model to integrate nitrogen transfers and transformations in rural landscapes. Environ Pollut. 159(11):3162–3170. doi: 10.1016/j.envpol.2011.05.005.

Elwan E, Le Page M, Jarlan L, Baghdadi N, Brocca L, Modanesi S, Dari J, Quintana Seguí P, Zribi M. 2022. Irrigation mapping on two contrasted climatic contexts using Sentinel-1 and Sentinel-2 data. Water. 14(5):804. doi: 10.3390/w14050804.

Gogé F, Thuriès L, Fouad Y, Damay N, Davrieux F, Moussard G, Roux CL, Trupin-Maudemain S, Valé M, Morvan T. 2021. Performance of near infrared spectroscopy of a solid cattle and poultry manure database depends on the sample preparation and regression method used. J Near Infrared Spectrosc. 29(4):226–235. doi: 10.1177/09670335211007543.

Guilayn F, Jimenez J, Martel J-L, Rouez M, Crest M, Patureau D. 2019a. First fertilizing-value typology of digestates: a decision-making tool for regulation. Waste Manag. 86:67–79. doi: 10.1016/j.wasman.2019.01.032.

Guilayn F, Jimenez J, Rouez M, Crest M, Patureau D. 2019b. Digestate mechanical separation: efficiency profiles based on anaerobic digestion feedstock and equipment choice. Bioresour Technol. 274:180–189. doi: 10.1016/j.biortech.2018.11.090.

Hafner SD, Pacholski A, Bittman S, Burchill W, Bussink W, Chantigny M, Carozzi M, Génermont S, Häni C, Hansen MN, et al. 2018. The ALFAM2 database on ammonia emission from field-applied manure: description and illustrative analysis. Agric For Meteorol. 258:66–79. doi: 10.1016/j.agrformet.2017.11.027.

Jouraiphy A, Amir S, El Gharous M, Revel J-C, Hafidi M. 2005. Chemical and spectroscopic analysis of organic matter transformation during composting of sewage sludge and green plant waste. Int Biodeterior Biodegrad. 56(2):101–108. doi: 10.1016/j.ibiod.2005.06.002.

Lashermes G, Nicolardot B, Parnaudeau V, Thuriès L, Chaussod R, Guillotin ML, Linères M, Mary B, Metzger L, Morvan T, et al. 2009. Indicator of potential residual carbon in soils after exogenous organic matter application. Eur J Soil Sci. 60(2):297–310. doi: 10.1111/j.1365-2389.2008.01110.x.

Malley DF, Martin PD. 2003. The use of near-infrared spectroscopy for soil analysis. In Tools for nutrient and pollutant management: application to agriculture and environmental quality, Occasional Report No. 17. Fertilizer and Lime ResearchCentre, Massey University, Palmerston North, New Zealand; p. 371–404.

Malley DF, Yesmin L, Eilers RG. 2002. Rapid analysis of hog manure and manure-amended soils using near-infrared spectroscopy. Soil Sci Soc Am J. 66(5):1677–1686. doi: 10.2136/sssaj2002.1677.
Maris SC, Abalos D, Capra F, Moscatelli G, Scaglia F, Cely Reyes GE, Ardenti F, Boselli R, Ferrarini A, Mantovi P, et al. 2021. Strong potential of slurry application timing and method to reduce N losses in a permanent grassland. Agric Ecosyst Environ. 311:107329. doi: 10.1016/j.agee.2021.107329.
Moinard V, Redondi C, Etiévant V, Savoie A, Duchene D, Pelosi C, Houot S, Capowiez Y. 2021. Short- and long-term impacts of anaerobic digestate spreading on earthworms in cropped soils. Appl Soil Ecol. 168:104149. doi: 10.1016/j.apsoil.2021.104149.
Möller K. 2015. Effects of anaerobic digestion on soil carbon and nitrogen turnover, N emissions, and soil biological activity. A review. Agron Sustain Dev. 35(3):1021–1041. doi: 10.1007/s13593-015-0284-3.
Odlare M, Pell M, Arthurson JV, Abubaker J, Nehrenheim E. 2014. Combined mineral N and organic waste fertilization – effects on crop growth and soil properties. J Agric Sci. 152(1):134–145. doi: 10.1017/S0021859612001050.
Ogen Y, Neumann C, Chabrillat S, Goldshleger N, Ben Dor E. 2018. Evaluating the detection limit of organic matter using point and imaging spectroscopy. Geoderma. 321:100–109. doi: 10.1016/j.geoderma.2018.02.011.
Pasquier C, Ayzac A, Carozzi M, Génermont S, Giot G, Yolaine G-D, Houot S, Moinard V, Voylokov P, Savoie A. 2019. Metametha dataset. doi: 10.15454/5MOZKJ.
Pastorelli R, Valboa G, Lagomarsino A, Fabiani A, Simoncini S, Zaghi M, Vignozzi N. 2021. Recycling biogas digestate from energy crops: effects on soil properties and crop productivity. Applied Sciences. 11(2):750. doi: 10.3390/app11020750.
Pedrayes OD, Usamentiaga R, Trichakis Y, Bouraoui F. 2023. Remote sensing for detecting freshly manured fields. Ecol Inf. 75:102006. doi: 10.1016/j.ecoinf.2023.102006.
Réveillé V, Mansuy L, Jardé É, Garnier-Sillam É. 2003. Characterisation of sewage sludge-derived organic matter: lipids and humic acids. Org Geochem. 34(4):615–627. doi: 10.1016/S0146-6380(02)00216-4.
Rienzi EA, Mijatovic B, Mueller TG, Matocha CJ, Sikora FJ, Castrignanò A. 2014. Prediction of soil organic carbon under varying moisture levels using reflectance spectroscopy. Soil Sci Soc Am J. 78(3): 958–967. doi: 10.2136/sssaj2013.09.0408.
Rivas H, Delbart N, Ottlé C, Maignan F, Vaudour E. 2021. Disaggregated PROBA-V data allows monitoring individual crop phenology at a higher observation frequency than Sentinel-2. Int J Appl Earth Obs Geoinf. 104:102569. doi: 10.1016/j.jag.2021.102569.
Romano E, Bergonzoli S, Bisaglia C, Picchio R, Scarfone A. 2023. The correlation between proximal and remote sensing methods for monitoring soil water content in agricultural applications. Electronics. 12(1):127. doi: 10.3390/electronics12010127.
Scarlat N, Dallemand J-F, Fahl F. 2018. Biogas: developments and perspectives in Europe. Renew Energy. 129:457–472. doi: 10.1016/j.renene.2018.03.006.
Shea K, Schaffer-Smith D, Muenich RL. 2022. Using remote sensing to identify liquid manure applications in eastern North Carolina. J Environ Manage. 317:115334. doi: 10.1016/j.jenvman.2022.115334.
Tang H, Qiu J, Van Ranst E, Li C. 2006. Estimations of soil organic carbon storage in cropland of China based on DNDC model. Geoderma. 134(1-2):200–206. doi: 10.1016/j.geoderma.2005.10.005.
THEIA-LAND. Données et services pour les surfaces continentales [accessed 2022 April 16] https://www.theia-land.fr/.
Vaudour E, Gholizadeh A, Castaldi F, Saberioon M, Borůvka L, Urbina-Salazar D, Fouad Y, Arrouays D, Richer-de-Forges AC, Biney J, et al. 2022. Satellite imagery to map topsoil organic carbon content over cultivated areas: an overview. Remote Sens. 14(12):2917. doi: 10.3390/rs14122917.
Vaudour E, Noirot-Cosson PE, Membrive O. 2015. Early-season mapping of crops and cultural operations using very high spatial resolution Pléiades images. Int J Appl Earth Obs Geoinf. 42:128–141. doi: 10.1016/j.jag.2015.06.003.
Vergnoux A, Guiliano M, Le Dréau Y, Kister J, Dupuy N, Doumenq P. 2009. Monitoring of the evolution of an industrial compost and prediction of some compost properties by NIR spectroscopy. Sci Total Environ. 407(7):2390–2403. doi: 10.1016/j.scitotenv.2008.12.033.
Verhoeven GJJ, Loenders J. 2006. Looking through black-tintedglasses—A remotely controlled infrared eye in the sky. In 2nd Int. Conf.Remote Sens. Archaeol. Proc. 2nd Int. Workshop—From Space to Place, Rome, Italy; p. 73–79.
Ward JH. 1963. Hierarchical grouping to optimize an objective function. J Am Stat Assoc. 58(301): 236–244. doi: 10.1080/01621459.1963.10500845.
Wentzel S, Schmidt R, Piepho H-P, Semmler-Busch U, Joergensen RG. 2015. Response of soil fertility indices to long-term application of biogas and raw slurry under organic farming. Appl Soil Ecol. 96: 99–107. doi: 10.1016/j.apsoil.2015.06.015.

WRB. 2015. World reference Base for soil resources 2014. World Soil Resources Reports (No. 106). FAO, Rome

Yu W, Hong Y, Chen S, Chen Y, Zhou L. 2022. Comparing two different development methods of external parameter orthogonalization for estimating organic carbon from field-moist intact soils by reflectance spectroscopy. Remote Sens. 14(6):1303. doi: 10.3390/rs14061303.

Zhang J, Wang X, Xue W, Xu L, Ding W, Zhao M, Liu S, Zou G, Chen Y. 2022. Microplastics pollution in soil increases dramatically with long-term application of organic composts in a wheat–maize rotation. J Clean Prod. 356:131889. doi: 10.1016/j.jclepro.2022.131889.

Zicker T, Kavka M, Bachmann-Pfabe S, Eichler-Löbermann B. 2020. Long-term phosphorus supply with undigested and digested slurries and their agronomic effects under field conditions. Biomass Bioenergy. 139:105665. doi: 10.1016/j.biombioe.2020.105665.

Žížala D, Minařík R, Skála J, Beitlerová H, Juřicová A, Reyes Rojas J, Penížek V, Zádorová T. 2022. High-resolution agriculture soil property maps from digital soil mapping methods, Czech Republic. CATENA. 212:106024. doi: 10.1016/j.catena.2022.106024.